Development of a system for simultaneous MRI and Near-infrared diffuse tomography to diagnose breast cancer

Ben A. Brooksby, Shudong Jiang, Gordon Ehret, Hamid Dehghani, Brian W. Pogue, Keith D. Paulsen
Thayer School of Engineering, Dartmouth College, Hanover NH 03755
(Email: brooksby@dartmouth.edu, Tel:(603) 646-1094, Fax:(603) 646-3856)

Astract: A multi-spectral, frequency-domain near infrared tomography system has been constructed and evaluated. Measurements of light transmission through female breast can be acquired simultaneously with MRI scans.

OCIS codes: (170.3830) Mammography; (170.6960) Tomography; (100.3010) Image reconstruction techniques

1. Introduction

Near infrared light can penetrate through tissue volumes of up to 12 cm, such as the female breast. Designing a system for imaging with sensitive optical detection instrumentation and an accurate model of diffuse light propagation, allows moderate resolution maps of tissue absorption and transport scattering coefficients (μ_a and μ_s') to be reconstructed[1]. A system which exploits the spectral dependence of light-tissue interaction can provide functional information, useful in diagnosing breast physiology and pathological state[2]. In an effort to improve sensitivity and specificity, spatial resolution and quantitative accuracy must be increased. It has been proposed that NIR image accuracy can be improved if *a priori* structural information is used to guide and constrain the iterative reconstruction process. Structural information could come from Ultrasound[3], X-ray mammography[4], CT or MRI[5, 6]. This work describes the design and performance of an optical tomography system capable of operating simultaneously with MRI. Results from phantom experiments suggest that *a priori* information, if used correctly, can significantly improve the accuracy of recovered optical properties.

2. System Design

This section describes the two elements that comprise the frequency-domain NIR tomography system, (1) light delivery and (2) detection. Both elements are mounted in a cart, shown in Figure 1(a), which can easily be transported to an MRI scanner for clinical studies.

2.1 Light delivery

The system deploys six laser diodes (660-850nm), which are amplitude modulated at 100 MHz by mixing a DC current source (ILX Lightwave) and an AC current from a frequency generator (IFR Systems). Each laser diode is held in a laser tube (THORLABS Inc.), and mounted on a linear translation stage (Velmex Inc.). This stage directs a specified wavelength into one of sixteen bifurcated optical fiber bundles (Ceramoptec Inc.). Each fiber is 13 meters in length and extends from the instrument cart, located outside of the MR suite, into the bore of the scanner (1.5T whole body imager, GE Medical Imaging Systems) to the patient interface.

The MR exam is performed using a Breast Array Coil (MRI Devices Corp.) that offers high-resolution imaging. The coil also provides an open architecture, which allows for the integration of a NIR-breast interface. A circular ring constructed of PVC guides the common end of each fiber into contact with the tissue surface. The fibers are evenly distributed around the circumference of tissue. Phosphor bronze compression springs (Ace Wire Spring & Form co., Inc.) maintain good fiber-tissue contact, and do not significantly deform the breast. The ring can be positioned such that the plane of measurements intersects the region of interest in tissue.

2.2 Light detection

For each source excitation, light transmission is recorded from 15 surface locations. This signal is measured by 15 PMTs (R6357, Hamamatsu Corp.) operating in parallel. The gain of the PMTs is varied to account for the large variation in light level between detectors depending on their distance from the source. The optimal gain levels are determined prior to each imaging series. Because each PMT is fixed to a particular fiber, it is necessary to switch gains electronically during the course of data collection. Upon assembly, these PMTs were optimized to achieve fast settling times after gain adjustment.

Electrical heterodyning through RF mixers is used to down convert the 100 MHz PMT signal to a lower frequency (500 kHz) which is filtered and amplified, then read by the computer. A PC running Labview software (National Instruments) is used to control all light delivery and detection equipment. Lock-in detection is used to extract log amplitude and phase data. For each wavelength, one imaging session yields this data for 240 source-detector pair locations. Including the time required to determine optimal gain values, acquisition takes about 1min.

3. Data Processing and Image Reconstruction

The data acquisition procedure involves important instrument calibration (1). Log amplitude and phase data are used in the (2) finite element analysis software to determine images of absorption and scattering.

3.1 Detector calibration and homogeneous phantom calibration

Each detector has a different amplitude and phase response to the same optical signal due to PMT variation, mixer performance, and fixed offsets in the RF splitter. A one-time calibration over the entire useful range of light levels and gains is applied[7]. A single source is placed in the center of a homogeneous diffusing object and measurements are obtained at each detector site. Each detector is exposed to the same optical signal, thus, the differences in log amplitude and phase are used as correction factors. The light intensity, but not phase, is changed by a series of neutral density filter wheels (New Focus). The amplitude and phase response of a representative PMT is shown in Figure 1(b) and (c) respectively. For a given gain setting, three values fully characterize PMT response: i) slope and ii) offset of log amplitude vs. input power, and iii) phase offset.

A final calibration is performed to account for offsets due to source fiber and detector fiber differences in transmission and alignment, as well as any errors in discretization or data/model mismatch. This involves a measurement from a homogeneous phantom[7]. When dealing with tissues having arbitrary shape, the effectiveness of the homogeneous phantom calibration hinges on the accurate specification of source and detector locations. We have fitted each fiber with a fiducial so that we can easily locate them in an MR image.

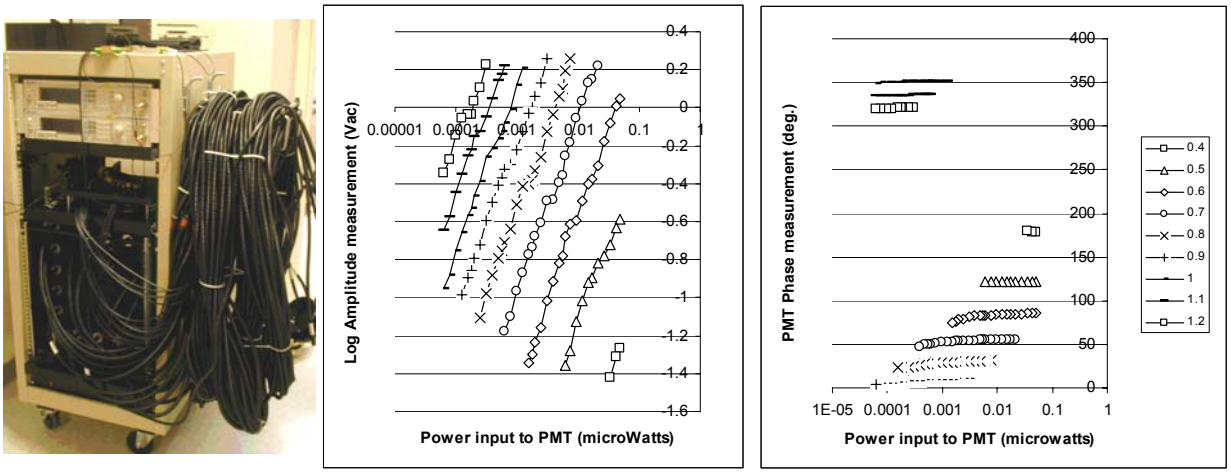

(a) **(b)** **(c)**

Figure 1. (a) The mobile NIR tomography system with long fibers for measurement inside the MRI. Graphs (b) and (c) show measurements used to calibrate a representative PMT. In (b) the Log Amplitude response is shown to be linear with input log of optical power. The phase response does not change significantly with input power changes, as long as the amplitude is within a linear range, with adequate signal to noise ratio.

3.2 FEM analysis

Data acquired from the detection system is processed by a FEM based reconstruction algorithm to generate tomographic images of absorption and scattering coefficient. The reconstruction algorithm exploits the frequency-domain diffusion equation approximation to light behavior in a highly scattering medium[1]. Methods of improving NIR reconstructions by incorporating MRI data have been explored in previous work[6, 8].

4. System Performance/Experimental Results

The lowest detectable signal occurs in the sub-picoWatt range. With a series of tissue-like phantom experiments, the measurement repeatability of the system as a whole has been characterized. The average RMS error at each detector site was determined to be 0.94% in AC intensity, and 0.85 degrees in phase. We have also performed more

critical tests of the instrument, through systematic acquisition of NIR data and MRI data on phantoms simultaneously, and have attempted to reconstruct high resolution, quantitatively accurate μ_a and μ_s' distributions.

Figure 2(a) shows a T1 weighted MRI slice of a cylindrical, gelatin phantom with optical properties similar to breast tissue (μ_a=0.0095 mm^{-1}, μ_s'=0.8 mm^{-1}, diam=82 mm). Visible in the image are the surface impressions caused by the optical fibers, and a ¼ wedge shaped inclusion with a higher absorption coefficient in order to mimic a tumor (μ_a=0.04 mm^{-1}, μ_s'=0.9 mm^{-1}). The MRI image was used to create a 2D finite element mesh that accurately represents the irregular phantom boundary in the plane of measurement. Figure 2(b) shows the standard NIR phantom reconstructions. The recovered peak values for the inclusion region, μ_a=0.025 mm^{-1} and μ_s'=2.57 mm^{-1}, are too low and too high respectively. Image artifacts, especially in μ_s' are also visible around the boundary. Next we used the MR to differentiate between the mesh points associated with the background and those within the inclusion region. By using a reconstruction algorithm described elsewhere[8], which exploits this information, and the benefits of parameter reduction, we reconstruct the images shown in Figure 2(c). Here, the recovered peak values for the inclusion region, μ_a=0.037 mm^{-1} and μ_s'=0.90 mm^{-1}, represent 92.5% and 100% accuracy, respectively.

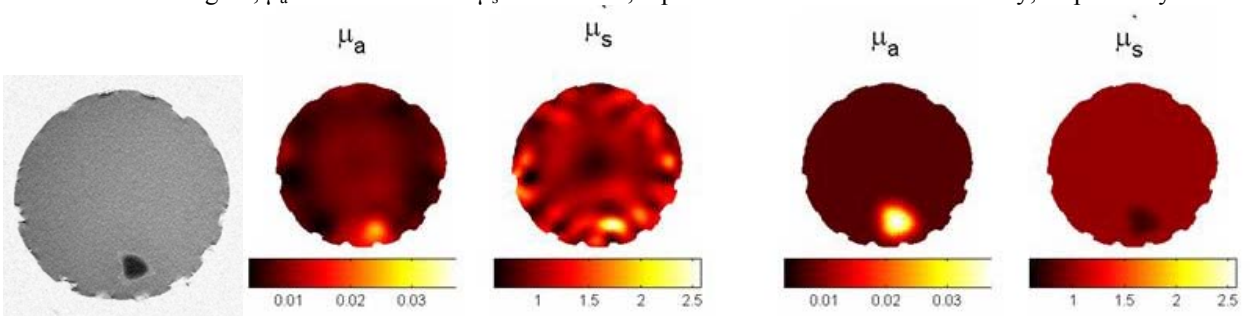

Figure 2. (a) T1 weighted MRI slice through cylindrical gelatin phantom. The inclusion, visible toward the bottom, has a higher absorption coefficient than the background (4:1). MR contrast was generated by adding $CuSO_4$. (b) shows absorption and scattering coefficient reconstructions on an FEM mesh which accurately represents the phantom shape as shown in (a). (c) shows the benefit of incorporating more *a priori* information from (a) into the iterative image reconstruction process. The size and shape of the inclusion were used to constrain optical property updates. Image accuracy improved, especially in quantitative recovery of μ_a for the inclusion.

5. Discussion

We have assembled an imaging system which can perform dual-modality NIR-MRI imaging of female breast tissue, and have used preliminary phantom studies to develop image reconstruction techniques for exploiting the benefits of its combined data set. NIR reconstruction is sensitive to any constraints applied to the spatial behavior of the diffusion model, and errors in such constraints can produce grossly inaccurate images. For the phantom test shown here, reconstruction of an absorbing inclusion improved by 30% when its size, shape, and location are accurately known. For more heterogeneous models, such as layered phantoms and *in vivo* breast tissue, it is likely that an MRI will offer comparable synergistic benefits.

6. Acknowledgements

This work has been sponsored by the National Cancer Institute through grants RO1CA78734 and PO1CA80139.

7. References

1. H. Dehghani, Pogue, B. W., Poplack, S. P., Paulsen, K. D. "Multiwavelength three-dimensional near-infrared tomography of the breast: initial simulation, phantom, and clinical results." Applied Optics, vol.42(1) pp. 135-145. 2003
2. S. Srinivasan, Pogue, B. W., Jiang, S., Dehghani, H., Kogel, C., Soho, S., Gibson, J. J., Tosteson, T. D., Poplack, S. P., Paulsen, K. D. "Interpreting hemoglobin and water concentration, oxygen saturation, and scattering measured *in vivo* by near-infrared breast tomography." Proc. Nat. Acad. Sci., vol.100(21) pp. 12349-12354. 2003
3. Q. Zhu, Chen, N. G., Kurtzman, S. H. "Imaging tumor angiogenesis by use of combined near-infrared diffusive light and ultrasound." Optics Letters, vol.28(5) pp. 337-339. 2003
4. A. Li, Miller, E. L., Kilmer, M. E., Brukilaccio, T. J., Chaves, T., Stott, J., Zhang, Q., Wu, T., Choriton, M., Moore, R. H., et al "Tomographic optical breast imaging guided by three-dimensional mammography." Applied Optics, vol.42(25) pp. 5181-5190. 2003
5. V. Ntziachristos, Yodh, A. G., Schnall, M. D., Chance, B. "MRI-Guided diffuse optical spectroscopy of malignant and benign breast lesions." Neoplasia, vol.4(4) pp. 347-354. 2002
6. B. W. Pogue, Zhu, H., Nwaigwe, C., McBride, T. O., Osterberg, U. L., Paulsen, K. D., Dunn, J. F. "Hemoglobin imaging with hybrid magnetic resonance and Near-Infrared Diffuse Tomography." Oxygen Transport to Tissue XXIV, pp. 215-224. 2002
7. T. O. McBride, Pogue, B. W., Jiang, S., Osterberg, U. L., Paulsen, K. D. "A parallel-detection frequency-domain near-infrared tomography system for hemoglobin imaging of the breast *in vivo*." Review of Scientific Instruments, vol.72(3) pp. 1817-1824. 2001
8. B. A. Brooksby, Dehghani, H., Pogue, B. W., Paulsen, K. D. "Near-infrared tomography breast image reconstruction with a priori structural information from MRI: algorithm development for reconstructing heterogeneities." IEEE JSTQE, vol.9(2) pp. 199-209. 2003.